Robust phase retrieval of complex-valued object in phase modulation by hybrid Wirtinger flow method

Zhun Wei[a,*], **Wen Chen**[b,c], **Tiantian Yin**[a], **Xudong Chen**[a]
[a]Department of Electrical and Computer Engineering, National University of Singapore, 117583, Singapore
[b]Department of Electronic and Information Engineering, The Hong Kong Polytechnic University, Hong Kong, China
[c]The Hong Kong Polytechnic University Shenzhen Research Institute, Shenzhen 518057, China

Abstract. A robust iterative algorithm, termed hybrid Wirtinger flow (HWF) method, for phase retrieval of complex objects from noisy diffraction intensities is presented. The results indicate that HWF method consistently outperforms the widely-used hybrid input-output and error reduction (HIO-ER) and oversampling smoothness (OSS) methods in terms of both accuracy and convergence rate in multiple phase modulations. The proposed algorithm is also more robust to low oversampling ratio, loose constraint, and noisy environment. Furthermore, compared with traditional Wirtinger flow (WF) method, the sample complexity is largely reduced without needing to adjust parameters case by case. It is expected that HWF will find applications in the rapidly growing coherent diffractive imaging (CDI) field for high-quality image reconstruction, as well as other disciplines where phase retrieval under phase modulation is needed.

Keywords: Coherence imaging, Phase retrieval, Phase modulation, Computational imaging.

***Zhun Wei,** eleweiz@nus.edu.sg

1 Introduction

Phase retrieval (PR), which aims to reconstruct an unknown signal or image from the phaseless measurements, plays an important role in both science and engineering. For example, in coherent diffractive imaging (CDI), it is used to reconstruct a noncrystalline specimen or a nanocrystal in nanometric scale resolution from the measured far-field diffraction intensity patterns.[1–3] In optical encryption systems, the PR technique is widely used to reconstruct phase only masks or original images.[4,5] To help solve the PR problem, modulator[6–9] has been introduced. Since several diffraction patterns can be recorded through phase modulation, the possibility of stagnation can be reduced in phase retrieval problems.

The first widely accepted method for phase retrieval is the alternating projection method proposed by Gerchberg and Saxton (GS),[10] which starts from a random initial guess and projects alternatively between frequency and time domain to update the current estimate. By applying

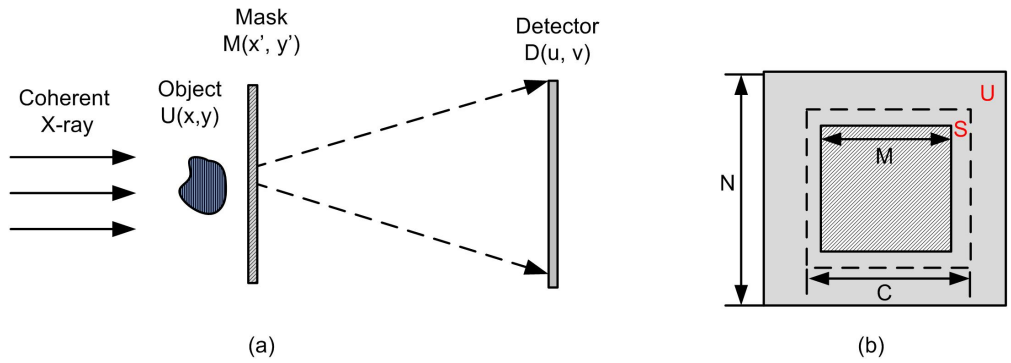

Fig 1 (a). Geometry for modulated coherent diffractive imaging; (b) Schematic of object plane, where the total reconstructed object, real image, and constraint dimensions are $N \times N$, $M \times M$, $C \times C$, respectively.

certain constraints, hybrid input-output method (HIO)[11] is proposed based on GS algorithm, and it may be the most widely used PR algorithms in CDI imaging. Over the years, some modified HIO algorithms such as hybrid input-output and error reduction (HIO-ER),[11] guided HIO,[13] difference map,[12] and oversampling smoothness (OSS)[14] are proposed. Among them, HIO-ER and OSS algorithms are widely used.[14,15] Nevertheless, all of these methods are difficult to ensure the convergence theoretically due to the use of projections onto nonconvex constraint set.[16,17] Thus, stagnation problem is still a great challenge for phase retrieval, especially for complex object under noisy environment, where a strong support constraint such as positive constraint is usually required.

Recently, some theoretically convergent algorithms have been proposed. One of the well-known method is PhaseLift. In PhaseLift, by using the lift technique of semi-definite programming (SDP), the non-convex problem is converted into a convex problems.[18] Nevertheless, due to the lift of matrix, the computational cost is high in PhaseLift. Later, Wirtinger flow (WF) algorithm has been reported and is proved to allow exact recovery of the phase from magnitude measurements.[19] Most importantly, the computational cost in WF method is largely reduced compared with PhaseLfit. Whereas, the WF method has two aspects which can be improved. The first is

the relative slow convergence rate, and the second is the high sample complexity which requires $O(n \log n)$ measurements to exactly recover a signal with n length. The high sample complexity means that it needs to collect around 13 diffraction patterns to recover a 500×500 dimensional image. Recently, to reduce the sample complexity and increase the convergence rate, improved algorithms have been proposed such as conjugate gradient Wirtinger flow (CGWF),[20] truncated Wirtinger flow (TWF),[21] reshaped Wirtinger flow (RWF),[22] truncated amplitude flow (TAF),[23] and incremental truncated Wirtinger flow (ITWF).[24] These methods can solve the issues to some extent, whereas the sample complexity is still high compared with practical requirement. Moreover, for algorithms like truncated Wirtinger flow (TWF), there are about four parameters that need to be tuned during optimization process, which makes the algorithm inconvenient for various cases.

In this paper, we propose a hybrid Wirtinger flow (HWF) method and present it under the framework of coherent diffractive imaging model. It is noted that HWF method can also work in other disciplines where phase retrieval is needed. The proposed method is compared with the widely used HIO-ER and OSS algorithms in terms of convergence rate, accuracy, and robustness to low oversampling ratio, loose constraint, and noisy environment.

2 Theory and methodology

In principle, the phase retrieval problems are related with the equation:

$$\mathbf{b} = |\mathbf{A}\mathbf{z}|^2 \tag{1}$$

where $\mathbf{z}$ is a complex signal to be recovered, $\mathbf{A}$ is the linear sampling matrix, and $\mathbf{b}$ is the magnitude squared observation of the linear measurement of any complex signal $\mathbf{z}$. Usually, the following

least-squared equation is used to solve $\mathbf{z}$:

$$min\ f(\mathbf{z}) = \frac{1}{2}(|\mathbf{Az}|^2 - \mathbf{b})^2 \tag{2}$$

2.1 Phase modulated coherent diffraction imaging

In this paper, we consider the phase modulated coherent diffraction imaging (PMCDI) model[2,3] to present our method. As is depicted in Fig. 1(a), a highly coherent beam of X-ray incidents upon the sample and a phase mask is introduced immediately behind sample. Various diffraction intensity patterns are collected on the detector at far field by changing or shifting the modulator. Due to the loss of phase information in diffraction patterns, a phase retrieval algorithm is needed to reconstruct the image of sample. In CDI, due to the oversampling in diffraction patterns, there is always a non-density region surrounding the electron density region of sample region. In this paper, as is illustrated Fig. 1(b), we assume that each diffraction pattern is sampled with a dimensional size of $N \times N$ and the image has a dimensional size of $M \times M$. Thus, a oversampling ratio σ can be calculated as $\sigma = N^2/M^2$.[25]

In PMCDI, for an arbitrary object matrix Z, the far-field diffraction pattern (Fraunhofer approximation) D_i corresponding to the ith phase mask M_i in PMCDI can be calculated as:

$$\mathbf{D_i} = |\mathcal{F}[\mathbf{Z} \circ \mathbf{M_i}]|^2 \ \ , i = 1, 2, ..., L \tag{3}$$

where "$\mathcal{F}$" and "$\circ$" denotes Fourier transform and Hadamard product, respectively. $\mathbf{D_i}$ can further be simplified as $\mathbf{D_i} = \mathbf{A_i z}$, where $\mathbf{A_i}$ is the corresponding linear transform matrix incorporating the Fourier transform and the ith phase mask. $\mathbf{z}$ is the vectorized form of $\mathbf{Z}$.

2.2 *The HWF framework*

To reconstruct a complex sample image $\mathbf{Z}$, collected diffraction patterns are first stored in a three dimensional matrix D with the size of $N \times N \times L$, where L is the total number of phase masks used in measurement. Then, hybrid Wirtinger flow (HWF) method is used to reconstruct the sample image. HWF method starts with an initialization $\mathbf{z_0}$ by spectral method, which is calculated the leading eigenvector of the matrix $\mathbf{A_i}^* \operatorname{diag}(\mathbf{z})\mathbf{A_i}$ by power iteration method with "$*$" denotes transpose conjugate.[19,21] Different from TWF,[21] constraint is applied in the object plane and the diffraction patterns are used one by one in the initialization process of HWF. The implementation procedures of initialization in HWF can be described as:

2.2.1 *Initialization*

- Step 1) $n = 1$ and $i = 1$, randomly generate a normalized signal $\mathbf{z_0}$. Then, obtain truncated diffraction patterns $\mathbf{D_t}$ with $\mathbf{D_t} = \mathbf{D} \circ \mathbf{\Gamma}\{\mathbf{D} \leq \alpha^2 t\}$, where Γ is a logical matrix with element being 1 when the condition $\mathbf{D} \leq \alpha^2 t$ is satisfied. t is the mean values of $\mathbf{D}$ and α is a constant parameter. Usually, α is around 2.5 empirically.

- Step 2) Calculate $\mathbf{z_0}' = \mathbf{A_i}^*(\mathbf{D_{ti}} \circ \mathbf{A_i z_0})$, where $\mathbf{D_{ti}}$ is the truncated diffraction pattern corresponding to ith mask.

- Step 3) Apply constraint and update $\mathbf{z_0}$: If $x \in S$, $\mathbf{z_0}(x) = \mathbf{z_0}'(x)$; If $x \notin S$, $\mathbf{z_0}(x) = \mathbf{z_0}'(x) - \beta \mathbf{z_0}'(x)$. Here, S represents a finite support as is depicted in Fig. 1(b) and β is a constant parameter between 0 and 1 ($\beta = 0.95$ is chosen in this paper).

- Step 4) Normalize $\mathbf{z_0}$. If $i = L$, go to step 5). Otherwise, let $i = i + 1$, and go to step 2).

- Step 5) If $n = M_{ite}$ ($M_{ite} = 20$ in this paper), stop iteration and $\mathbf{z_0} = \sqrt{t}\mathbf{z_0}$. Otherwise, let $n = n + 1$ and $i = 1$, and go to step 2).

2.2.2 Optimization direction and stepsize

In the optimization process, HWF iteratively updates $\mathbf{z_{k+1}}$ through the following equation:

$$\mathbf{z_{k+1}} = \mathbf{z_k} - \alpha_k \mathbf{l_k} \tag{4}$$

with $k = 0,\ 1,\ 2,\ ....$ Polak-Ribière-Polyak (PRP) direction[26] is used as the search direction $\mathbf{l_k}$ to accelerate the convergence rate.[20] Specifically, Wirtinger derivative at nth iteration d_k is firstly calculated as $\mathbf{d_k} = \mathbf{A}^*((|\mathbf{A}\mathbf{z_k}|^2 - \mathbf{D}) \circ \mathbf{A}\mathbf{z_k})$. Here, the linear operator $\mathbf{A}$ incorporates all the results of L $\mathbf{A_i}$ operators into a three dimensional matrix, and $\mathbf{A}^*$ conducts a mean operation for all L $\mathbf{A_i^*}$ operators. Then, the PRP direction $\mathbf{l_k}$ is calculated as follows: If $k = 0$, $\mathbf{l_k} = \mathbf{d_k}$. Otherwise,[27]

$$\mathbf{l_k} = \mathbf{d_k} - (\mathrm{Re}[\mathbf{d_k}^* \cdot (\mathbf{d_k} - \mathbf{d_{k-1}})]/||\mathbf{d_{k-1}}||^2)\mathbf{l_{k-1}} \tag{5}$$

with "$||\cdot||$" and "Re" being Euclidean norm and taking real part, respectively.

The stepsize α_k is calculated as the real roots of a univariate cubic equation:[25,28]

$$a_c\alpha_k^3 + b_c\alpha_k^2 + c_c\alpha_k + d_c = 0 \tag{6}$$

where the constant coefficients $a_c = \sum_{i=1}^{m} |\mathbf{h_i}|^4$, $b_c = -3\sum_{i=1}^{m} \mathbf{u_i} \circ |\mathbf{h_i}|^2$, $c_c = \sum_{i=1}^{m} \mathbf{r_i} \circ |\mathbf{h_i}|^2 + 2\mathbf{u_i}^2$, and $d_c = -\sum_{i=1}^{m} \mathbf{u_i} \circ \mathbf{r_i}$ with $\mathbf{h_i} = \mathbf{A}\mathbf{l_k}$, $\mathbf{u_i} = \mathrm{Re}(\mathrm{conj}(\mathbf{A}\mathbf{z_k}) \circ \mathbf{h_i})$, and $\mathbf{r_i} = |\mathbf{A}\mathbf{z_k}|^2 - \mathbf{D}$.[28] Here, "conj" means taking conjugate.

Fig 2 Original (a) magnitude and (b) phase of the object to be reconstructed.

2.2.3 Implementation procedures of HWF

The complete implementation procedures of HWF algorithm for CDI application are described as follows:

- Step 1) Initial step, $k = 0$; Calculate the initial value $\mathbf{z}_0$ based on the power iteration method.
- Step 2) Determine the search direction according to Eq. (5).
- Step 3) Determine the search length α_k according to the real roots in Eq. (6).
- Step 4) Update $\mathbf{z_{k+1}}$: Calculate $\mathbf{z'_k} = \mathbf{z_k} - \alpha_k \mathbf{l}_k$. If $x \in S$, $\mathbf{z_{k+1}}(x) = \mathbf{z'_k}(x)$; If $x \notin S$, $\mathbf{z_{k+1}}(x) = \mathbf{z'_k}(x) - \beta \mathbf{z'_k}(x)$.
- Step 5) If termination condition such as reaching a maximum iterations is satisfied, stop iteration. Otherwise, let $k = k + 1$, and go to step 2).

3 Results

In this section, we conduct numerical experiments to compare the proposed method with the widely used HIO-ER and OSS methods in terms of convergence speed and accuracy of reconstructed

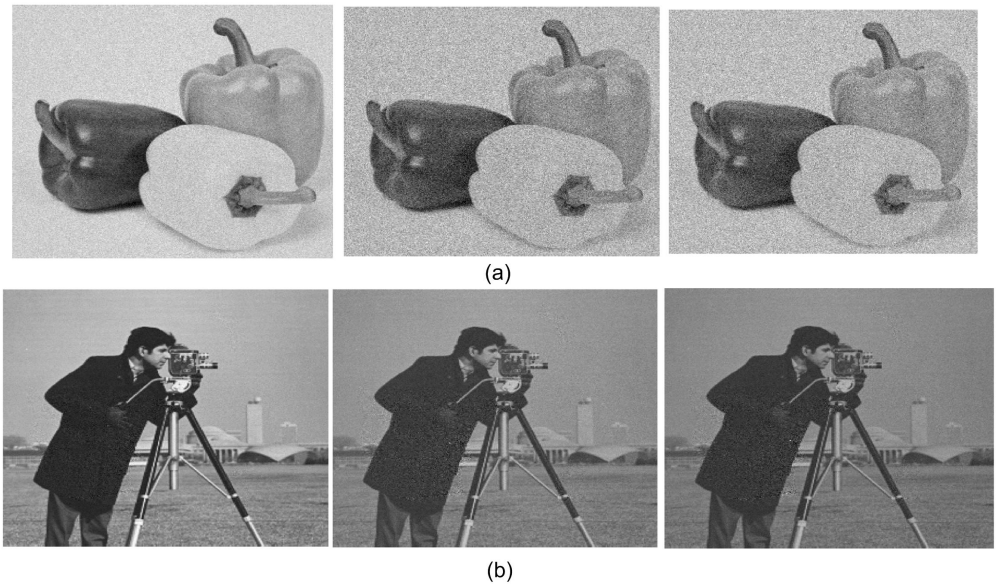

Fig 3 (a) Recovered magnitude and (b) Recovered phase with noise ratio $R_n = 15\%$ (From left to right: HWF, HIO-ER, and OSS). For HWF method, the results are from 150th iteration. For HIO-ER and OSS, the results are from 1000th and 2000th iteration, respectively.

results. As is depicted in Fig. 1(b), We consider an object with $N = 500$, and a complex image with $M = 300$ is inserted in the object to model the practical oversampling in experiment. The original magnitude and phase of the complex image $\mathbf{Z}$ is presented in Fig. 2(a) and 2(b), respectively. To reconstruct the object image, a total number of $L = 3$ diffraction patterns are collected, which is much smaller than the patterns needed in traditional WF method. Tight constraint ($M = C$) is conducted in the numerical analysis unless otherwise stated. In all the results, Poisson noise $\mathbf{n}$ is added to the diffraction patterns $\mathbf{D}$, and is quantified by noise ratio $R_n = (||\mathbf{n}||_F/||\mathbf{D}||_F) \times 100\%$ with $||\cdot||_F$ denotes Frobenius norm. Besides the visual quality of the reconstructed image, normalized mean square error (NMSE) is also defined to quantitatively evaluate the reconstructed image:

$$NMSE = ||\mathbf{Z_k} - \mathbf{Z}||_F^2/||\mathbf{Z}||_F^2 \tag{7}$$

Table 1 Iterations and NMSEs under different noise, constraint, and oversampling ratios for HWF, HIO-ER, and OSS methods (NC means not convergent). It is noted that the NMSE of OSS is still slowly decreasing after 2000 iterations.

		HWF		HIO-ER		OSS	
		Iteration	NMSE	Iteration	NMSE	Iteration	NMSE
$\rho = 0\%$, $\sigma = 2.78$	$R_n = 10\%$	20	0.057	300	0.12	2000	0.12
	$R_n = 15\%$	20	0.1	400	0.2	2000	0.2
	$R_n = 20\%$	20	0.13	1700	0.25	2000	0.25
$R_n = 15\%$ $\sigma = 2.78$	$\rho = 10\%$	25	0.1	1500	0.21	NC	NC
	$\rho = 20\%$	30	0.1	NC	NC	NC	NC
$R_n = 15\%$ $\rho = 0\%$	$\sigma = 2$	25	0.11	2300	0.21	NC	NC
	$\sigma = 1.56$	120	0.14	NC	NC	NC	NC

where Z_k is the restored object at kth iteration and Z are the original complex object. It should be noted that Z_k is multiplied by a constant value to get the rid of effect of constant phase shift.

3.1 Effects of noisy ratio

Figs. 3(a) and 3(b) present the reconstructed object magnitude and phase for HWF, HIO-ER, OSS methods with $R_n = 15\%$, respectively. For HIO-ER and OSS method, we run a total number of 1000 and 2000 iterations, respectively, unless no apparent change occurs between current and last step of the reconstructed image. For HWF method, a maximum number of 150 iterations is set. It is found that the results of reconstructed image for HWF methods are much better than those of the other two methods.

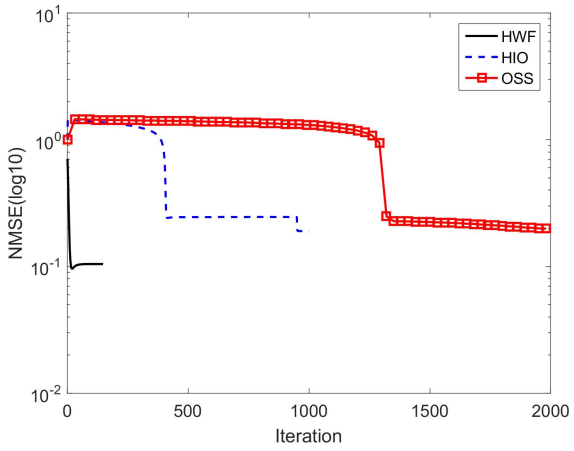

Fig 4 The NMSEs vary with iteration number for HWF, HIO-ER, and OSS methods with 15% noise.

To quantitatively compare the three methods, NMSEs are plotted in Figs. 4 when 15% noise presented. It can be seen that HWF converges to the minimum point with NMSE around 0.1 at about 20th iteration. Whereas, it takes much more iterations for both HIO-ER and OSS method to converge to a solution. Specifically, HIO-ER takes hundreds of iterations to converges to a minimum point with NMSE around 0.2 and OSS takes more than a thousand iterations to reach to a NMSE value around 0.2. It is also noted that the NMSE of OSS is still slowly decreasing after 2000 iterations. These results suggest that the reconstructed results of HWF method are quantitatively much better than those of the other two methods. Furthermore, consider that the computational complexities of three methods at each iteration are very close, HWF are also much faster than HIO-ER and OSS. In the first three row of Table 1, the iterations needed and NMSE for three methods are further compared under different noise ratios. It is found that the noise ratio almost has no effects on the convergence rate of HWF but can affect the final NMSEs. Furthermore, it can be seen that HWF outperforms the other two methods in terms of both convergence speed and accuracy.

3.2 Effects of loose constraints and oversampling ratio

Practically, such as in CDI, one can hardly know the exact boundary of the sample when conducting phase retrieval. Thus, loose constraints ($C > M$) are normally used. To explore the effects of loose constraints on the proposed HWF method, constraint ratio $\rho_c = (C^2 - M^2)/M^2$ is defined, where $\rho_c = 0$ corresponds to the tight constraint. Figs. 5(a) and 5(b) present the reconstructed object magnitude and phase for HWF, HIO-ER, OSS methods with a quite loose constraint ratio $\rho_c = 20\%$, respectively. It is found that the both HIO-ER and OSS can hardly converges, and only very obscure images are observed in the results of reconstructed phase. Whereas, for HWF, high

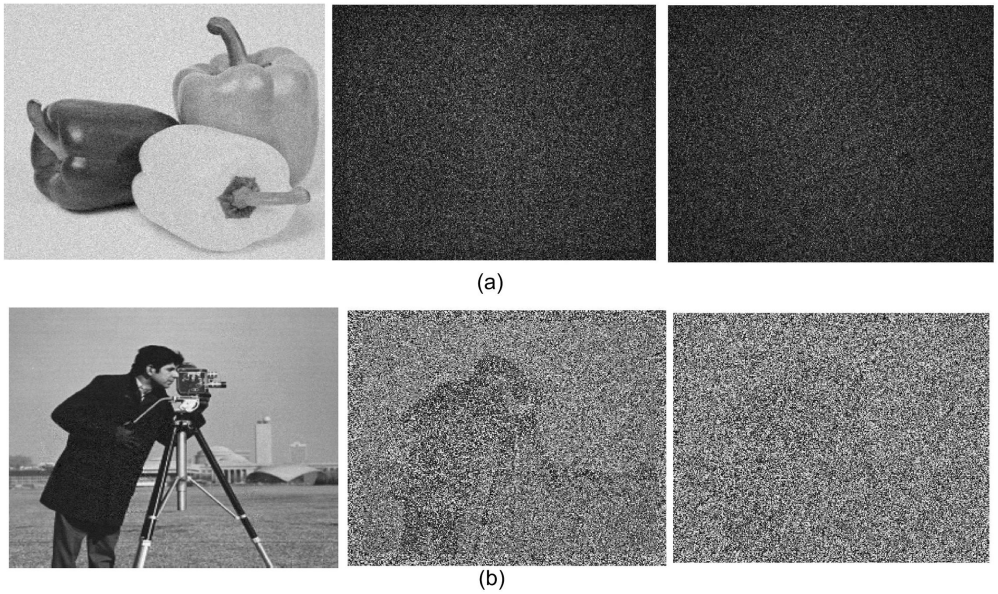

Fig 5 (a) Recovered magnitude and (b) Recovered phase with loose constraint ratio ($\rho_c = 20\%$) (From left to right: HWF, HIO-ER, and OSS). For HWF method, the results are from 150th iteration. For HIO-ER and OSS, the results are from 1000th and 2000th iteration, respectively.

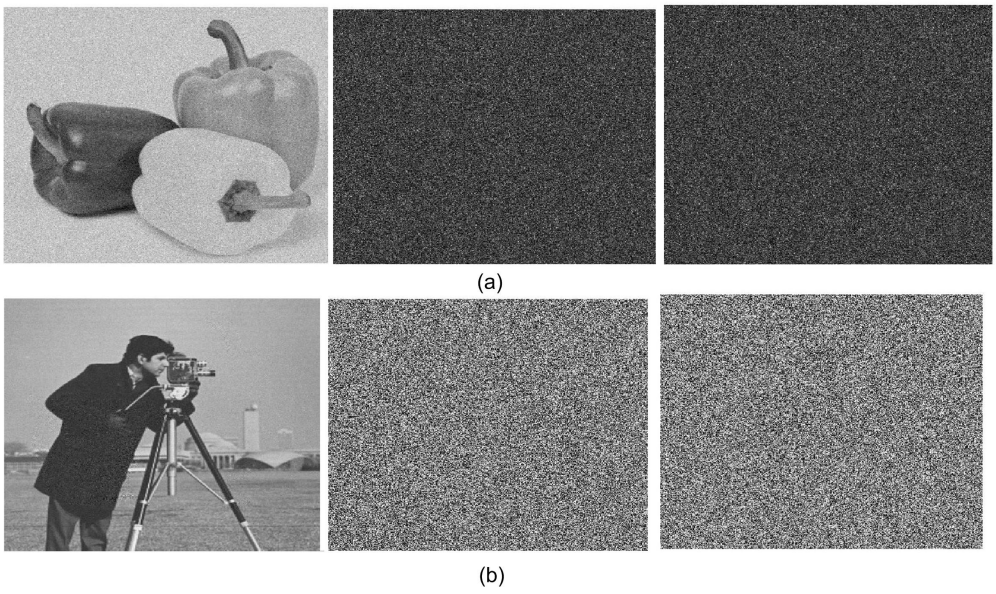

Fig 6 (a) Recovered magnitude and (b) Recovered phase with low oversampling ratio ($\sigma = 1.56$) (From left to right: HWF, HIO-ER, and OSS). For HWF method, the results are from 150th iteration. For HIO-ER and OSS, the results are from 1000th and 2000th iteration, respectively.

quality reconstructed results are obtained.

In Figs. 6(a) and 6(b), the reconstructed magnitude and phase corresponding to a low oversampling ratio ($\sigma = 1.56$) are also presented. To change the oversampling ratio, only the size of

the real image (M) is changed and the total size of the object (N) is kept invariant. It can be seen that, with low oversampling ratio, HWF method is still able to reconstruct the complex object with high quality. Whereas, HIO-ER and OSS don't converge. In the last four rows of Table 1, the effects of loose constraint and low oversampling ratios are compared among the three methods. It is noted that the constraint ratio has small effect on convergence rate of HWF method, whereas the convergence rate is largely reduced for low oversampling ratio case. The results also show that the proposed HWF method is much more robust to both of loose constraint and low oversampling ratios compared with HIO-ER and OSS method.

3.3 Discussions

It is interesting and worthwhile to discuss the reasons behind the results in Figs. 3-6 and Table 1. For HIO-ER and OSS methods in multiple phase modulations, diffraction patterns are used one by one in the optimization process. At each iteration, $\mathbf{Z_{k+1}}$ is actually updated according to the Lth diffraction pattern, and the effects of other $L-1$ diffraction patterns are alleviated to some extend. Therefore, the methods are not accurate. For HWF method, due to the careful selection rule and constraint application in the spectral method, a noise robust initialization close to the solution is obtained with a low sample complexity. Moreover, diffraction patterns are used one by one in the initialization process to further reduce the sample complexity. Based on the initialization, constraint conjugate gradient approach is used in optimization process to accelerate convergence rate. In the optimization process, the search direction is updated according to the mean gradient of all diffraction patterns, which ensures the accuracy of the reconstruction results.

4 Conclusion

A constraint hybrid Wirtinger flow (HWF) method is presented in this paper. In HWF, constraints in CDI is combined with a new initialization process and conjugate gradient. Numerical results show that, comparing with HIO-ER and OSS algorithms in multiple phase modulations, the proposed HWF method is much faster and more accurate. Furthermore, the proposed HWF method is much more robust to loose constraints, low oversampling ratio, and noisy environments. As for the disadvantage of the proposed HWF method, our further simulations show that the proposed method can hardly converges to a solution for single shot ($L = 1$) imaging since a single diffraction pattern can hardly make the initialization process of HWF converge to a point near the solution.

Acknowledgments

This research was supported by the National Research Foundation, Prime Minister's Office, Singapore under its Competitive Research Program (CRP Award No. NRF-CRP15-2015-03). The support from Shenzhen Science and Technology Innovation Commission (Basic Research Program) under Grant No. JCYJ20160531184426473 is also acknowledged.

References

1 J. Miao, P. Charalambous, J. Kirz, and D. Sayre, "Extending the methodology of X-ray crystallography to allow imaging of micrometre-sized non-crystalline specimens," Nature 400, 342-344 (1999).

2 M. H. Seaberg, A. dAspremont, and and J. J. Turner "Coherent diffractive imaging using randomly coded masks," Appl. Phys. Lett. 107, 231103 (2015).

3 F. Zhang, G. Pedrini, and W. Osten, "Phase retrieval of arbitrary complex-valued fields through aperture-plane modulation," Physical Review A 75, 043805 (2007).

4 H. Di, Y. Kang, Y. Liu, and X. Zhang, "Multiple image encryption by phase retrieval," Optical Engineering 55(7), 073103 (2016).

5 W. Chen, X. Chen, and C. J. R. Sheppard, "Optical image encryption based on diffractive imaging," Opt. Lett. 35, 3817-3819 (2010).

6 F. Zhang, B. Chen, G. R. Morrison, J. Vila-Comamala, M. Guizar-Sicairos, and Ian K. Robinson, "Phase retrieval by coherent modulation imaging," Nat. Commun. 7, 13367 (2016).

7 X. Zhang, J. Jiang, B. Xiangli, and G. R. Arce, "Spread spectrum phase modulation for coherent X-ray diffraction imaging," Opt. Express 23, 25034-25047 (2015).

8 I. Johnson, K. Jefimovs, O. Bunk, C. David, M. Dierolf, J. Gray, D. Renker, and F. Pfeiffer, "Coherent diffractive imaging using phase front modifications, "Phys. Rev. Lett. 100(15), 155503 (2008).

9 F. Zhang, G. Pedrini, and W. Osten, "Phase retrieval of arbitrary complex-valued fields through aperture-plane modulation," Phys. Rev. A 75(4), 043805 (2007).

10 R. W. Gerchberg, "A practical algorithm for the determination of phase from image and diffraction plane pictures," Optik 35, 237 (1972).

11 J. R. Fienup, "Phase retrieval algorithms: a comparison," Appl. Opt. 21, 2758-2769 (1982).

12 V. Elser, "Solution of the crystallographic phase problem by iterated projections," Acta Crystallographica Section A: Foundations of Crystallography 59, 201-209 (2003).

13 C.-C. Chen, J. Miao, C. W. Wang, and T. K. Lee, "Application of optimization technique to

noncrystalline x-ray diffraction microscopy: Guided hybrid input-output method," Phys. Rev. B 76, 064113 (2007).

14 J. A. Rodriguez, R. Xu, C.-C. Chen, Y. Zou, and J. Miao, "Oversampling smoothness: an effective algorithm for phase retrieval of noisy diffraction intensities," J. Appl. Cryst. 46, 312-318 (2013).

15 Y. Shechtman, Y. C. Eldar, O. Cohen, H. N. Chapman, J. Miao, and M. Segev, "Phase retrieval with application to optical imaging: a contemporary overview," IEEE Signal Processing Magazine 32, 87-109 (2015).

16 S. Marchesini, "Invited article: A unified evaluation of iterative projection algorithms for phase retrieval," Rev. Sci. Instrum. 78, 011301 (2007).

17 Heinz H. Bauschke, Patrick L. Combettes, and D. Russell Luke, "Hybrid projection-reflection method for phase retrieval," J. Opt. Soc. Am. A 20, 1025-1034 (2003).

18 E. J. Candes, Y. C. Eldar, T. Strohmer, and V. Voroninski, "Phase retrieval via matrix completion," SIAM Rev. 57, 225-251 (2015).

19 E. J. Candes, X. Li, and M. Soltanolkotabi, "Phase retrieval via Wirtinger flow: Theory and algorithms," IEEE Transactions on Information Theory 61, 1985-2007 (2015).

20 Z Wei, W. Chen, C.-W. Qiu. and X. Chen, "Conjugate gradient method for Phase retrieval based on Wirtinger derivative," J. Opt. Soc. Am. A 34, 708-712 (2017).

21 Y. Chen and E. Candes, "Solving random quadratic systems of equations is nearly as easy as solving linear systems," Advances in Neural Information Processing Systems 28, 739-747 (2015).

22 H. Zhang, Y. Zhou, Y. Liang, and Y. Chi, "Reshaped Wirtinger Flow and Incremental Algorithm for Solving Quadratic System of Equations," arXiv preprint arXiv:1605.07719 (2016).

23 G. Wang, G. B. Giannakis, and Y. C. Eldar, "Solving systems of random quadratic equations via truncated amplitude flow," arXiv preprint arXiv:1605.08285 (2016).

24 R. Kolte and A. Ozgur, "Phase retrieval via incremental truncated Wirtinger flow," arXiv preprint arXiv:1606.03196 (2016).

25 J. Miao, T. Ishikawa, E. H. Anderson, and K. O. Hodgson, "Phase retrieval of diffraction patterns from noncrystalline samples using the oversampling method," Phys. Rev. B 67, 174104 (2003).

26 E. Polak and G. Ribière, "Note sur la convergence de methodes de directions conjuguees," Revue francaise informatique et de recherche operationnelle, serie rouge 3, 35-43 (1969).

27 P. M. van den Berg, A. L. van Broekhoven, and A. Abubakar, "Extended contrast source inversion," Inv. Probl. 15, 1325-1344 (1999).

28 X. Jiang, S. Rajan, and X. Liu, "Wirtinger Flow Method With Optimal Stepsize for Phase Retrieval," IEEE Signal Processing Letters 23, 1627-1631 (2016).